Desalination and Water Treatment
www.deswater.com

doi: 10.5004/dwt.2017.20863

80 (2017) 1–10
June

Biofouling patterns in spacer-filled channels: high-resolution imaging for characterization of heterogeneous biofilms

Marc Staal[a,§], Nadia Farhat[b,*,§], Mark van Loosdrecht[a], Johannes Vrouwenvelder[a,b]

[a]*Department of Biotechnology, Faculty of Applied Sciences, Delft University of Technology, Van der Maasweg 9, 2629 HZ Delft, The Netherlands, emails: staal.marc@gmail.com (M. Staal), M.C.M.vanLoosdrecht@tudelft.nl (M. v. Loosdrecht), J.S.Vrouwenvelder@tudelft.nl (J. Vrouwenvelder)*

[b]*Division of Biological and Environmental Science and Engineering (BESE), Water Desalination and Reuse Center (WDRC), King Abdullah University of Science and Technology (KAUST), Thuwal 23955-6900, Saudi Arabia, Tel. +966562604415, emails: nadia.farhat@kaust.edu.sa (N. Farhat), johannes.vrouwenvelder@kaust.edu.sa (J. Vrouwenvelder)*

[§]*Both authors contributed equally to this work.*

Received 22 March 2017; Accepted 22 April 2017

ABSTRACT

Biofilms develop in heterogeneous patterns at a μm scale up to a cm scale, and patterns become more pronounced when biofilms develop under complex hydrodynamic flow regimes. Spatially heterogeneous biofilms are especially known in spiral wound reverse osmosis (RO) and nanofiltration (NF) membrane filtration systems used for desalination and wastewater reuse to produce high quality (drinking) water. These spiral wound membrane modules contain mesh-like spacer structures used to create an intermembrane space and improve water mixing. Spacers create inhomogeneous water flow patterns resulting in zones favouring biofilm growth, possibly leading to biofouling thus hampering water production. Oxygen sensing planar optodes were used to visualize variations in oxygen decrease rates (ODR). ODR is an indication of biofilm activity. In this study, ODR images of multiple repetitive spacer areas in a membrane fouling simulator were averaged to produce high resolution, low noise ODR images. Averaging 40 individual spacer areas improved the ODR distribution image significantly and allowed comparison of biofilm patterning over a spacer structure at different positions in an RO filter. This method clearly showed that most active biofilm accumulated on and in direct vicinity of the spacer. The averaging method was also used to calculate the deviation of ODR patterning from individual spacer areas to the average ODR pattern, proposing a new approach to determine biofilm spatial heterogeneity. This study showed that the averaging method can be applied and that the improved, averaged ODR images can be used as an analytical, in-situ, non-destructive method to assess and quantify the effect of membrane installation operational parameters or different spacer geometries on biofilm development in spiral wound membrane systems characterized by complex hydrodynamic conditions.

Keywords: Desalination; Biofouling; Sensor; Non-destructive; Feed spacer; Spiral wound

1. Introduction

Biofilms, defined as a community of bacterial cells attached to surfaces in a matrix of extracellular polymeric substances, are considered as the prevalent bacterial mode of existence in nature [1,2]. Biofilms develop in heterogeneous distribution patterns, and the attachment and subsequent growth of bacteria on a surface is influenced by several factors including mainly hydrodynamics, biochemical gradients, and surface physical properties. Spatial variations in hydrodynamic conditions affect the distribution of biofilm at a mesoscale level (mm–cm) [3]. The initial deposition of

* Corresponding author.

bacterial cells on a surface is not only affected by the bacterial cell properties (e.g., size, charge and hydrophobicity) [1,4] but also by local hydrodynamic conditions like shear stress and hydraulic retention, influencing bacterial cell adherence to the surface and detachment [5]. After an initial attachment phase, bacterial cells start to divide, and cell division will contribute increasingly to biofilm development. At a certain point, growth by cell division (converting nutrients into biomass) will become the dominant biomass accumulation process and this will result in an exponential increase in biomass amount until biodegradable nutrient transport processes become limiting. The local nutrient flow through the biofilm, mainly by diffusion, determines the nutrient supply to the biofilm and thereby the growth of the biofilm.

Drinking water production increasingly depends on membrane treatment processes such as reverse osmosis (RO) and nanofiltration (NF) [6]. However, biofouling occurrence remains the primary concern that hinders the application of these membrane filtration processes [7]. RO/NF membrane treatment systems include feed spacer structures which affect the hydrodynamic conditions inside the filtration modules. Feed spacers are used to create a flow channel space between two membrane sheets in the spiral wound membrane elements required for water transport. The spacers improve water mixing thus reducing the overall diffusive boundary layer thickness as well as reducing concentration polarization [8] improving the treatment efficiency. Feed spacers can have different designs (e.g., geometries) but generally have a mesh-like structure with mesh sizes of 2–3 mm [9,10]. One main problem is the feed spacer's sensitivity to undesired biofilm growth (biofouling), reducing the water production efficiency of membrane systems significantly [11–13]. The morphology and spatial orientation of the feed spacer affect the bacterial deposition patterns [5] and thereby partly determine the biofilm distribution in later growth phases. Flow cells with flat surfaces and laminar flow conditions are commonly used to study submerged biofilms under water flow [14]. Only a few studies have been performed addressing biofilm spatial distribution patterns in systems that include physical obstacles to the water flow such as the feed spacers; thereby generating variable hydrodynamic conditions [5,15–17].

Light and confocal microscopes significantly improved our understanding of biofilm structure and population dynamics at a μm to mm scale and provided us with the familiar biofilm image consisting of pillars and mushroom-like structures separated by voids or water-filled channels [18]. However, microscopic techniques give limited information on spatial biofilm development variability at mm to cm scale, which is specifically needed in membrane systems containing spacers with mesh sizes of 2–3 mm and complex hydrodynamics such as in RO/NF spiral wound membrane systems. Two and three-dimensional modelling can describe the interaction of flow, biodegradable nutrient transport, and bacterial growth at mm scale [19], but modelling has computational limitations when the studied areas require modelling of several centimetres at high resolution.

With the development of planar optodes, measuring the spatial distribution of oxygen at mm to cm scale in-situ, non-destructively became possible. Planar optodes consist of an oxygen-sensitive luminescent dye fixed in a polymeric matrix [20,21]. The luminescence intensity or lifetime optode images are indicative of the oxygen concentration and can be measured with a CCD camera. Most studies with oxygen sensing optodes focused on the description of vertical oxygen gradients in sandy sediments by placing the optodes in contact with existing equilibrated sediments [22,23]. Only a few studies described the development of biofilm structures by growing the biofilm on top of the optode [24,25]. Steady-state oxygen distribution depends on several parameters such as diffusive boundary layer thickness, volumetric oxygen respiration, and biomass thickness. Since no vertical gradients are measured, it is a challenge to estimate these parameters. Therefore, Farhat et al. [16] applied the oxygen sensing planar optodes to visualize variations in oxygen decrease rates (ODRs) which are considered to be indicative of biofilm activity. ODRs are more informative for the description of bacterial presence and activity than oxygen distribution under steady-state conditions [16]. Using the ODR technique, biofilm development patterns in single spacer frame units as well as over the whole membrane fouling simulator (MFS) could be visualized. The signal/noise ratio in the mentioned studies required digital filtering to better visualize ODR patterns; however, digital filtering reduces the sharpness of edges of the ODR pattern. In addition, the variation between ODR patterns between different individual spacer frames was high; therefore, comparing different areas in the MFS unit using general descriptive parameters like overall ODR values and oxygen depletion was only possible without taking into account the variation at mm scale. Overall ODR and oxygen depletion values do not describe variation between different spacer frames nor describe the overall spatial distribution patterns of biofilms caused by the spacer geometry. Recently, a new tool was developed to analyze spatial distribution patterns of groups of bacteria in highly heterogeneous biofilms based on one-dimensional sectioning to determine an average noise threshold based on repetitive spatial structures on a mm scale [26,27]. This new tool improved quantifying the vertical distribution and the co-aggregation patterns of defined biofilm populations [26,27]. However, for imaging ODR patterning in a fouling flow cell, containing a spacer, this type of analysis cannot be used since the patterns are two-dimensional and not one-dimensional like the data in the Daims and Wagner studies [27]. Therefore, a two-dimensional imaging analysis method is required to determine an average biofilm distribution pattern per spacer area.

In this study, oxygen sensing planar optodes were used to image two areas of the MFS (inlet side, first 4 cm; outlet side, last 4 cm) to visualize the variation in biofilm activity measured in-situ, non-destructively through the ODR. The imaged areas contained repetitive spacer frame structures, and 40 spacer frame structures were averaged to reconstruct a high-resolution ODR image with relatively low signal to noise levels. The average ODR image was used to show local deviation in biofilm patterning over individual spacer areas by comparing the ODR of each spacer area with the calculated average ODR. Comparison of ODR pattern in individual spacer areas with the average ODR pattern allows precise analysis of overall spatial changes in ODR distribution patterns (biofilm patterning) over a period of time. To the best of our knowledge, this type of averaging of repetitive structures is used for the first time in biofilm research and

this averaging method provided high-resolution information on biofilm spatial formation under complex hydrodynamic conditions.

2. Materials and methods

A detailed description of the experimental setup, imaging method, and oxygen distribution determination can be found in [16]. In short, biofilms were grown in an MFS with a transparent window. The MFS contains a 20 cm × 4 cm coupon of a membrane and a feed spacer [28]. The feed spacer was a 31 mil (787 μm) thick diamond-shaped polypropylene spacer (porosity 0.85). Fig. 1 shows the feed spacer orientation used in this experiment (45° contact angle with feed flow, as commonly used in spiral wound membrane elements). Hydrodynamic conditions in the MFS were similar to spiral wound membrane modules as applied in practice for water treatment [28]. The MFS was operated without permeate production at a pressure of 1 bar. Earlier studies done with membrane elements in the same position in NF and RO installations, with and without permeate production, showed the same development of pressure drop increase and biofilm formation [29].

The system was run as a continuous flow reactor. Tap water (24°C) was pumped through the MFS at 16 $L \cdot h^{-1}$, which equals a standard flow velocity of 0.16 $m \cdot s^{-1}$, representative for practice [29]. A nutrient stock solution containing sodium acetate, sodium nitrate, and sodium phosphate in a mass ratio C:N:P of 100:20:10 was added to the feed water increasing the feed water nutrient concentration by 1 mg $C \cdot L^{-1}$ to enhance biofilm formation in the MFS.

Oxygen distribution at the first 4 cm (inlet side) and the last 4 cm (outlet side) of the 20 cm long MFS was measured daily for 4 d with oxygen-sensitive luminescent optodes. Apogee imaging systems (Ascent A285 CCD Camera, 1,392 pixels × 1,040 pixels, 16 bit) with a Nikon Nikkor 35 mm f/1.4 lens and a bandpass filter (690–850 nm, Astrodon photometrics, Sloan photometric filters i'2) was used to take luminescence images from the optode. A Nikon macro extension ring shortened the focal distance to 15 cm, depth of field 1.9–2.2 mm, and a pixel size of 45 μm × 45 μm. The oxygen sensing dye used in the planar optode was based on the dye PtTPTBPF (excitation 595 nm, emission 775 nm) immobilized in a polystyrene matrix (4% w/w PE/chloroform) [30]. The dye was excited by amber LEDs (1 W lumiled, 595 nm) placed around the camera lens. The power supply for the LEDs was a laboratory power supply (AIM-TTI instruments, PL303), providing a stable output. The MFS and the camera system were placed in a light-tight box to minimize the effect of external light on the luminescence images.

Spatial oxygen distribution was calculated with a luminescence intensity imaging approach [25]. Image processing was performed in ImageJ (version 1.49 m). The ODR was determined using a stop-flow imaging protocol. The stop-flow imaging protocol consisted of (i) a dark intensity image, (ii) the stop-flow image series, and (iii) the anaerobic intensity image [16]. The dark intensity image was subtracted from all intensity images to eliminate the background effect. The stop-flow image series consisted of a sequence of 100 intensity images taken at 6 s intervals. The anaerobic luminescence intensity image was made after the stop-flow images by pumping of a concentrated solution of sodium hydrosulfite (20 $g \cdot L^{-1}$) into the MFS feed water at a rate of 0.125 $mL \cdot h^{-1}$. The anaerobic luminescence intensity image was taken once a day and sodium hydrosulfite consumed all oxygen present in the monitor. The stack of the stop-flow intensity image series was divided by the anaerobic intensity image where

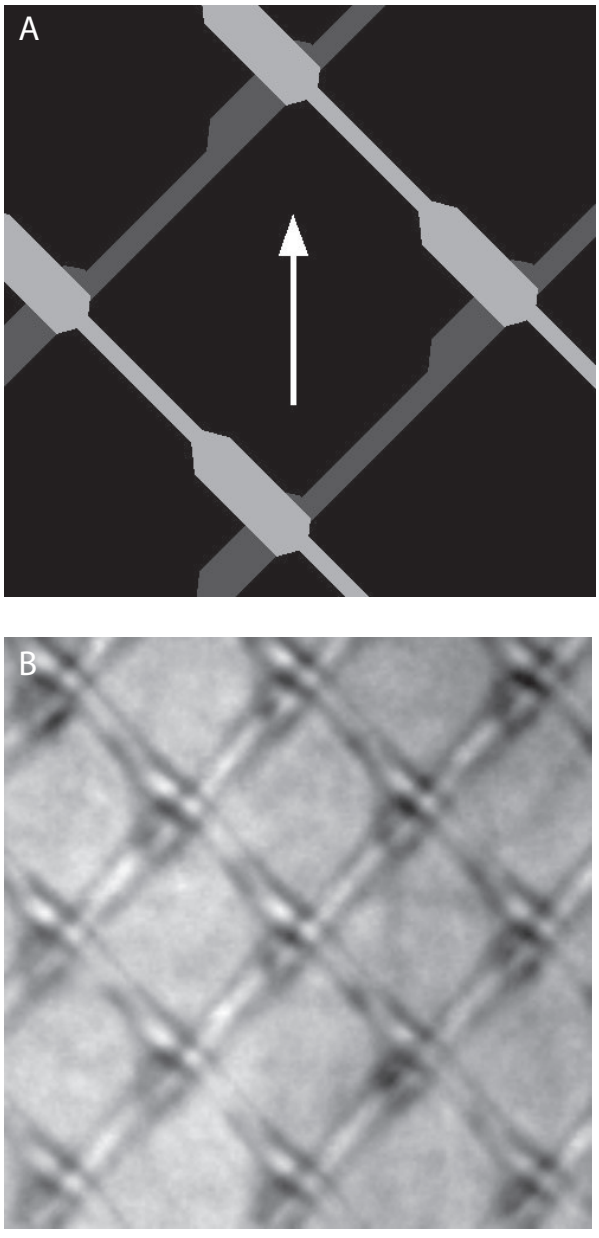

Fig. 1. (A) Schematic drawing of the feed spacer. The light grey area indicates the spacer strands that are touching the optode (\-orientation). The dark grey area indicates the spacer strands that are under the light grey strands touching the membrane. The dark grey spacer strands are situated further away from the optode (/-orientation). The larger distance between the spacer and the optode allows a higher water passage. The thin areas of the spacer strand allow more water passage than the thick areas. The white arrow indicates the average flow direction. The spacer configuration is equal to configuration D2 in [5]. (B) An area of the spacer at a smaller magnification.

after the ratio images were converted into a stack of O_2 concentration images using Stern–Volmer equation [16].

An area of 4 cm × 4 cm was imaged per oxygen image. One image included approximately 110–130 individual spacer frames. The first step was to make a stack (S1) containing three images: one anoxic intensity image, and two aerobic intensity images from a stop-flow series (one aerobic intensity image at t = 0 and one at t = 30 s after stopping the water flow). The three images in stack S1 were all positioned at exactly the same position. Positioning the three images on top of each other before cropping guaranteed that the same areas were selected for calculation of both oxygen images.

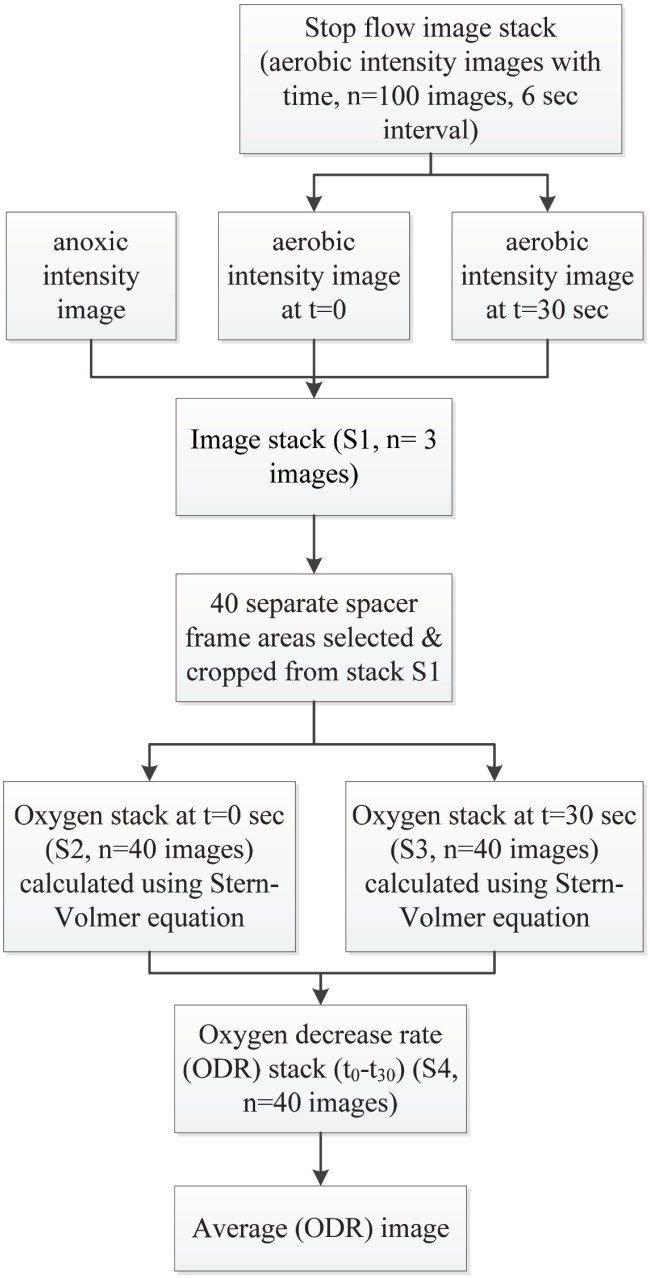

Fig. 2. Flow chart scheme describing the image processing steps to obtain an average ODR image over a spacer frame area.

40 separate areas were manually selected and cropped from stack S1. For these 40 areas, the oxygen images were calculated using the aerobic intensity images and anoxic image based on the Stern–Volmer equation determined from calibration. As a result two oxygen image stacks (S2, S3) were determined, S2 at t = 0 and S3 at t = 30 s each oxygen image stack containing n = 40 images resembling the 40 cropped areas. From stacks S2 and S3, ODR stack was determined (S4). Average ODR images were calculated from these stacks. For clarity image size was increased (500 pixels × 500 pixels) using the linear interpolation option in imageJ and false colouring was applied. A contour of the feed spacer was added to the images to indicate where the feed spacer strands were situated.

3. Results

Biofilm formation was monitored daily over a period of 4 d. During these 4 d averaged ODR images were calculated to visualize overall changes in spatial ODR patterns at the inlet (Fig. 3) and outlet (Fig. 4) region of the MFS. An average ODR of about zero mg $O_2 \cdot L^{-1} \cdot s^{-1}$ was observed at the start of the experiment on day 0. The colour scale of the ODR images was optimized per day to increase the contrast in the individual images allowing comparison of the ODR patterns for the consecutive days. On day 1, spatial ODR patterns were already visible in the averaged images while no structuring was visible in the non-averaged images (data not shown). A region with an increased ODR was found under the spacer strand with the \-orientation (Figs. 3 and 4). On day 2, the ODR under the other spacer strand (/-orientation) increased but did not reach ODR values as high as under the \-spacer strand yet. Differences in maximum ODR between the spacer strands of different orientation were almost absent at day 3, though the /-spacers had a wider region with an elevated ODR. At day 3, a channel with a lower ODR became clearly visible under the /-spacer. This channel was also visible at day 4. Day 4 was also the day at which the ODR under the /-spacer strand became higher than ODR under the \-spacer strands. The regions where the spacer strand physically touched the optode (the thicker part of the \-spacer strand) did not develop a high ODR over the whole experimental period.

In conclusion, the regions of the spacer where the biofilm on the initial days started to develop and showed the highest ODR changed in time. Spacer regions touching the membrane had lowest ODR on the initial days, however, showed the highest ODR on day 4.

At first sight, little difference in the average ODR patterns was observed between the inlet and outlet region (Figs. 3 and 4) and the overall ODR values of the whole image (Fig. 6) did not differ. However, one visible difference is the wider water flow channel under the /-orientated spacer strand at the outlet. Also the area with the higher ODR under the /-oriented spacer seems wider especially at the downstream side of the spacer strand.

The ratio of the ODR images from the MFS inlet and outlet was determined to better visualize the differences between the inlet and outlet regions of the MFS (0–4 cm and 16–20 cm) (Fig. 5). Values below zero (black and dark blue) indicate the areas with a higher ODR in the outlet and values above

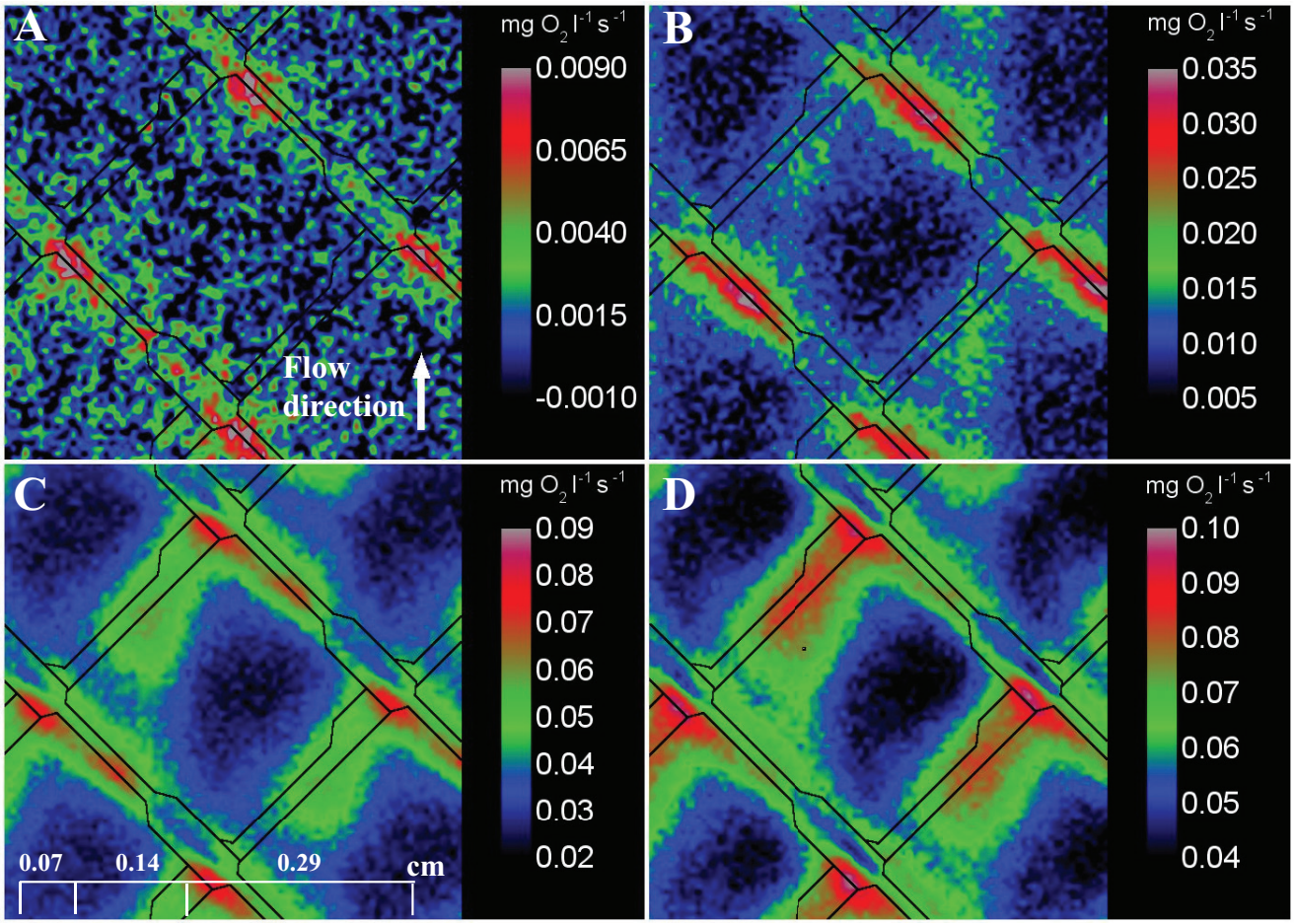

Fig. 3. Average oxygen decrease rates (ODR in mg $O_2 \cdot L^{-1} \cdot s^{-1}$) ($n$ = 40) at the inlet side (0–4 cm) of the membrane fouling simulator (MFS) in four consecutive days (day 1–4). The drawn structure indicates the position of the feed spacer. Feed water at a velocity of 0.16 m s^{-1} flows from bottom to top. The color scales are different for all days to improve contrast in the image to allow comparison of the oxygen structures between the different days of the biofilm study.

zero indicate (green, yellow, and red) the areas where the inlet showed a higher ODR. The highest differences between inlet and outlet were observed at day 2 and the differences decreased at day 3 and day 4. Fig. 5 shows the regions where the biofilm patterning at the inlet differed from the outlet. The centre of a spacer compartment had a higher ODR in the outlet, while the \-spacers showed a higher ODR at the inlet at day 4.

Using ODR images, it is also possible to quantitatively average the ODR in selected regions of interest (ROIs). The ODR was zero at the start of the study when no biofilm was present (day 0) and increased with time during the 4-day experiment (Fig. 6). The highest ODR values were found in the regions situated under the spacer. Initially (day 1–3) the ODR was highest under the spacer strands that are in direct contact with the optode (\-orientation, red areas). At day 4 the highest ODR is found under the spacer strand located further away from the optode (/-orientation, blue areas). The maximum ODR values were ~0.11 mg $O_2 \cdot L^{-1} \cdot s^{-1}$. The ODR in central region (green area) was almost half of the values found under the spacer regions. In summary, biofilm mainly developed on or in the direct vicinity of the feed spacer.

4. Discussion

The main objectives of this biofilm study in spacer-filled flow channels were to evaluate whether averaging repetitive structures imaged by oxygen planar optodes result in high-resolution spatial ODR images suitable to study spatial variations in distribution of biofilms under variable hydrodynamic conditions. The oxygen planar optodes provided spatially-resolved ODR (measure for biofilm activity) showing that most active biofilm accumulation occurred on and in direct vicinity of the spacer over the membrane fouling simulator length (Figs. 3–5), with most biomass under the feed spacer strands (Fig. 6). Novelty of the results is the ability to differentiate biofilm development on the different spacer strands and its change in time. High resolution, low noise ODR images were obtained by averaging a high number of spacer areas (Figs. 3–7), enabling the quantification of spatial biofilm activity distribution (Table 1).

4.1. Averaging to visualize spatial biofilm patterning

Hydrodynamic conditions affect biofilm spatial patterning mainly by controlling two interlinked

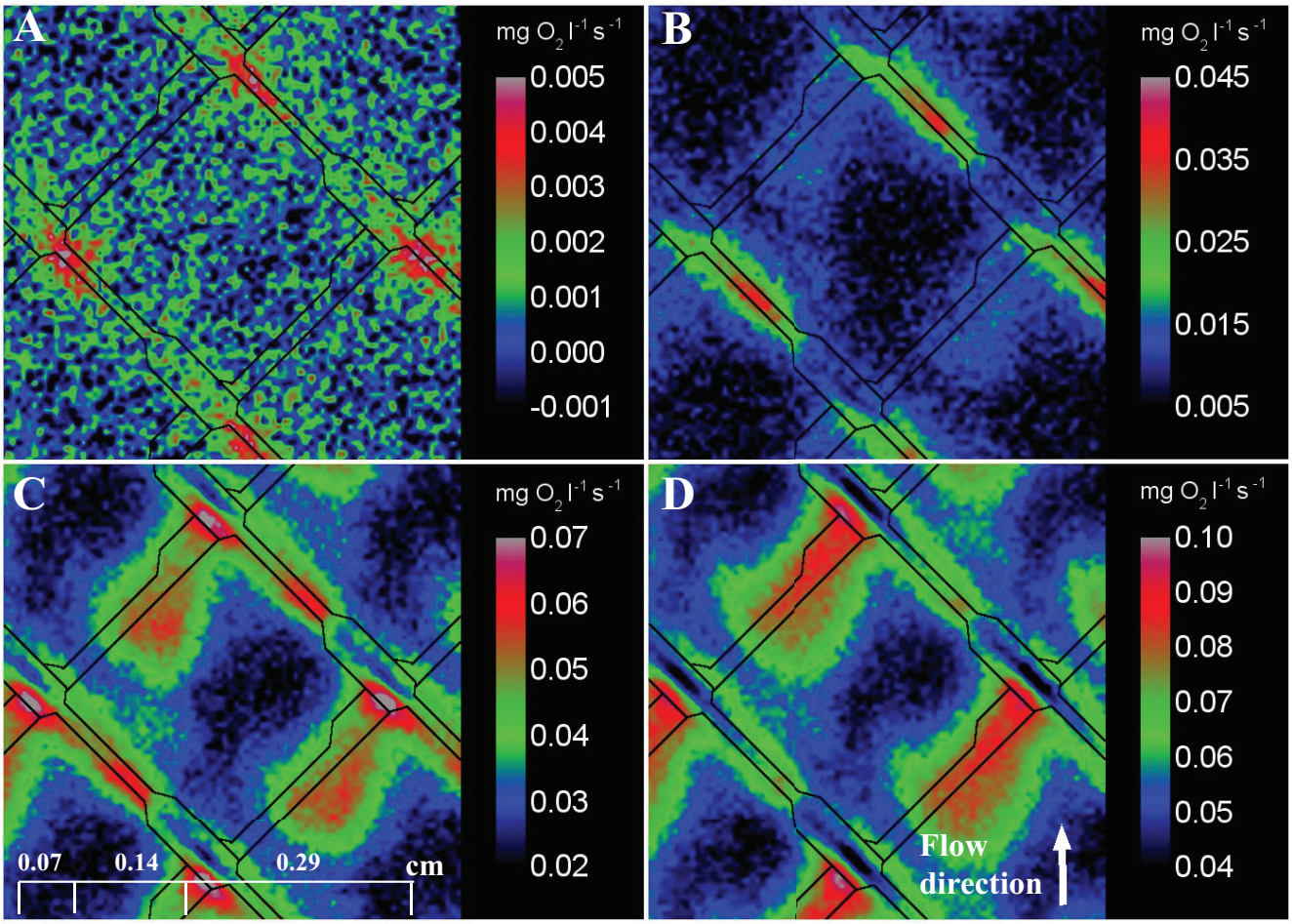

Fig. 4. Average oxygen decrease rates (ODR in mg $O_2 \cdot L^{-1} \cdot s^{-1}$) ($n$ = 40) at the outlet side (16–20 cm) of the MFS in four consecutive days (day 1–4). The drawn structure indicates the position of the spacer. Feed water at a velocity of 0.16 m s^{-1} flows from bottom to top. The color scales are different for all days to improve contrast in the image to allow comparison of the oxygen structures between the different days of the biofilm study.

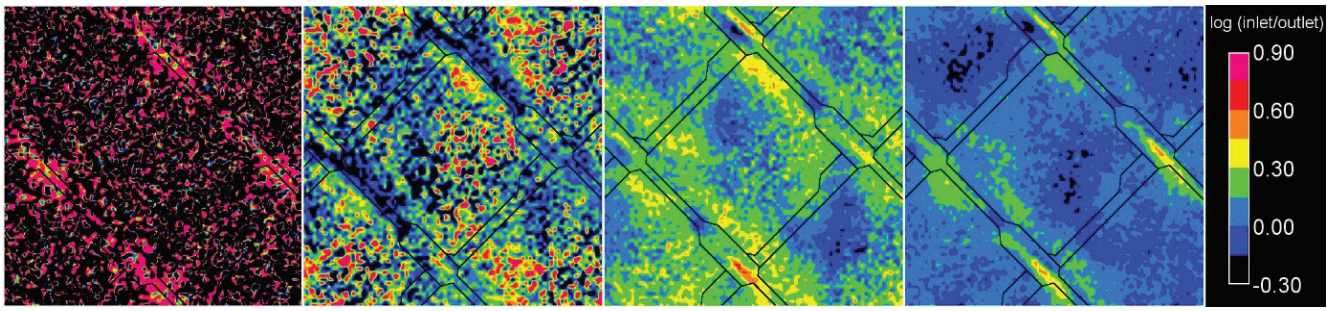

Fig. 5. The log transformed ratio images calculated by division of the average inlet ODR image by the average outlet ODR image (n = 40). Values below zero represent a higher activity at the outlet while values above zero represent a higher biofilm activity in the inlet.

parameters: nutrient mass transfer and shear force [31]. Biofilms grown under laminar conditions form patchy and roughly circular bacterial cell clusters separated by interstitial voids while biofilms grown under turbulent conditions form patches of ripples and elongated "streamers" during the initial and exponential growth phase [24,32,33]. The presence of the feed spacer structures in the flow field results in variability in the flow pattern and affects the rate and distribution of bacterial attachment/detachment [5] as well as bacterial cell growth. Growth will vary due to variations in nutrient fluxes and shear stress as a result of variable hydrodynamic conditions.

In this study, the average ODR of the total inlet and outlet image (110–130 spacer frames) showed an exponential increase with time. Little variation was observed in the average ODR values between the MFS inlet area and the outlet

side. However, the variation in ODR spatial distribution patterns between single feed spacer frames is high. Therefore, it is not possible to compare individual spacer frames from inlet and outlet side of the MFS directly. Averaging spacer frames could overcome the high variability observed between single spacer areas and will result in an average ODR image with high resolution. It is expected that the variation in biofilm distribution within the total single spacer frame will determine the number of images to be averaged for the generation of a high-resolution average image. In this study, it was found that averaging of 40 individual spacer frames resulted in the highest resolution average ODR image. From the initial imaged area (4 cm × 4 cm) containing approximately 110–130 individual spacer frames, a maximum of 40 single spacer frame images without overlapping areas could be cropped. A lower number of averaged single spacer frame areas (n) already gave a good indication of the overall contours of the biofilm structure (Fig. 7) but at $n \leq 10$ the resulting average image has a relatively low resolution and is not suitable for a good comparison of different regions within the MFS. At $n = 10$, the resulting average image has a better resolution; however, the spatial distribution in the average image changes when any random 10 single spacer frame images are taken for averaging. Therefore, the resulting average ODR spatial pattern at $n = 10$ differed from $n = 20$ and $n = 40$. This difference is due to high variability in biofilm development between the single feed spacer frames, especially at the inlet side (see also section 4.2). Minor difference in spatial distribution of the ODR pattern was observed when averaging 20 or 40 cropped spacer frame areas. Hence, with heterogeneity in biofilm distribution as found in this study a minimum of 20 single spacer frame images is required to generate an illustrative average image for the ODR distribution.

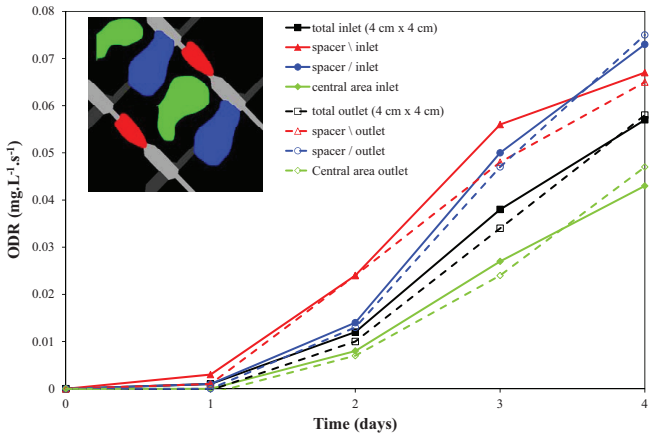

Fig. 6. Average oxygen decrease rates (ODR in mg $O_2 \cdot L^{-1} \cdot s^{-1}$) ($n = 40$) at the inlet and outlet side of the MFS in four consecutive days. The colored structure indicates the ROI positions relative to the spacer. Feed water at a velocity of 0.16 m s^{-1} flows from bottom to the top. The ODR values of ROI's of equal colours are averaged over the 40 single spacer frames. Average ODR values of the total imaged area (4 cm × 4 cm, black lines) are also calculated.

4.2. Analysis of spatial patterns of biofilms

In this study, the \-spacer surprisingly developed a higher ODR than the /-spacer at the initial stages. The \-spacer is the spacer situated closest to the oxygen sensing optode, and the opening between that spacer strand and the optode reduced water passage between the optode and the spacer. Thus, the local lower water flow conditions resulted in a higher initial net attachment rate and a higher initial growth, despite an expected lower nutrient mass transfer. The increase in ODR under the \-spacer was exponential for the first 3 d but started to level off at day 4. The stabilization in ODR development at day 4 indicates that the biofilm in between the \-spacer and the optode began to become limited in growth at day 4, probably due to limitation in the transfer of biodegradable nutrients. The ODR under the /-spacer had a slower initial development when compared with the ODR under the \-spacer. Figs. 3 and 6 show that the area with the highest ODR was in the middle of that spacer strand for both the inlet and the outlet. Differences between the inlet and the outlet were also found, which can partly be explained by the initial attachment of bacterial cells. Deposition patterns on the membrane were found in particle attachment studies done by [5]. Radu et al. [5] found that particles similar in size as bacterial cells flowing through spacer frames resulted in regions with relatively higher particle attachment rates. The regions with the highest attachment rates were the regions that had the highest local shear [5] specifically underneath the spacer filament and nearby similar to the results reported in this study. However, only the attachment rate by abiotic particles was simulated by Radu et al. [5] and did not include biological growth.

In this study, it was shown that despite the big differences in distribution patterns per spacer frame, averaged spatial ODR patterns were visible at the mm scale. This

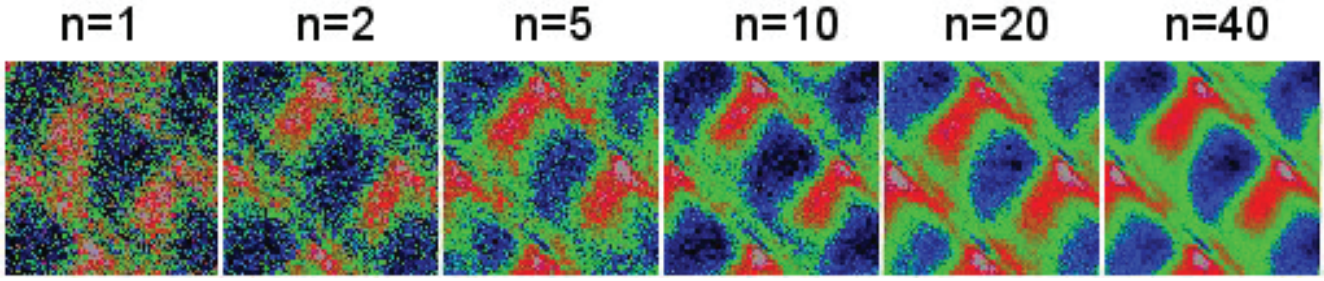

Fig. 7. Effect of spacer frame number averaging on the ODR distribution image in the MFS inlet. The number of spacer frame images averaged is indicated above the images.

Table 1
Standard deviation calculated from the total ODR image from the inlet and outlet (600 pixels × 500 pixels) after smoothing using a mean filter (radius 1 pixel) in imageJ. The deviation from the average image is calculated from the batch of 40 images (85 pixels × 85 pixels, see supplementary material)

Day	Standard deviation		Deviation from average image	
	Inlet	Outlet	Inlet	Outlet
0	0.0156	0.0159	0.254	0.259
1	0.0161	0.0159	0.256	0.243
2	0.0160	0.0167	0.259	0.255
3	0.0203	0.0186	0.361	0.278
4	0.0213	0.0186	0.410	0.295

allowed visualization and detailed quantitative analysis of spatial ODR patterns that are not visible in the non-averaged images. This will give new insight in overall developing mechanisms of biofilms in RO filtration systems that contain spacers with specific geometries. The biofilm that formed in the tested spacer configuration will influence flow patterns in the spacer frames but also in between frames since differences in biomass and flow pattern between frames will create preferential water flow channels. It can be anticipated that a developing biofilm at an early stage would start to influence hydrodynamics and thereby start to engineer its surroundings. An example of this bioengineering is the flow channel formation found in the area where the spacer strands cross, for example, on the left side of the image (Figs. 4 and 5). The water has to pass through the spacer-filled channel somewhere, and it may be the channel where most water passes as a result of the biofilm growth elsewhere. Picioreanu et al. [34] showed that biofilms can form mushroom-like structures with voids in between at a μm scale mainly under nutrient-limited conditions. Later on, the presence of voids may improve overall nutrient mass transport into the biofilm by creating convection flow into the biofilm [33]. Dynamic changes in flow channel patterns over time caused by this process has been reported [35].

4.3. Heterogeneity in biomass distribution

Heterogeneity in biomass distribution can be described by determining the standard deviation of the image [36] or with roughness (a normalized standard deviation) [37]. However, the standard deviation as a heterogeneity indicator assumes a random distribution and does not take into account the occurrence of hydraulic flow patterns as an important environmental factor affecting the spatial biofilm development. In membrane filtration systems including a feed spacer, it can be assumed that part of the spatial biofilm heterogeneity is caused by the presence of the feed spacer and the other part is a result of the position where the measurements are performed, for example, the inlet vs. outlet side. Averaging the images of the single feed spacer frames allows discriminating the effect of the presence of the spacer on spatial biofilm heterogeneity from the effect of spatial location on heterogeneity (inlet and outlet) when comparing biofilm development at two locations (e.g., inlet side and outlet side). The deviation of individual images from the average image (e.g., 40 images) can be calculated (Fig. S1). The individual spacer frames at the inlet side deviated more from the average image (Table 1) in comparison to the outlet. This deviation may be used as a measure for inter-spacer frame variability. At the outlet, there was almost no increase in the standard deviation of spatial biofilm distribution over time. The difference in deviation from the average image between the inlet and the outlet side is most probably caused by trapping larger-sized bacterial cell aggregates at the inlet region compared with the outlet. Trapping bigger cell aggregates will result in a more rapid and stronger spatial heterogeneity in biofilm distribution [38] and may also explain the differences found in the averaged spatial patterning images between the inlet and the outlet.

5. Conclusions

Spatially-resolved oxygen decrease rates, a measure for biofilm activity made during in-situ, non-destructive biofilm imaging studies of spacer-filled flow channels, were used to analyze the locations of biofilm development, to evaluate a new method based on averaging of repetitive spatial structures for spatial biofilm characterization. Based on the results of membrane fouling simulator studies presented in this article, it can be concluded that:

- High resolution, low noise oxygen decrease rates images were obtained by averaging individual spacer areas, enabling visualization of overall spatial biofilm distribution. This novel method to visualize in-situ, non-destructively the spatial development of biofilm patterns shows that repetitive feed spacer frame structures can serve to improve oxygen decrease rates images by averaging the regions that have the same physical spacer structure. Averaging can overcome inter-compartmental variability between spacer frames and thus can be used for analyzing the effect of physical structures on biofilm formation in general and specifically the effect of spacer geometry on local fouling patterns. The resulting average images enabled the (i) comparison of biofilm patterning between two locations in the membrane fouling simulator and the (ii) characterization of biofilm spatial heterogeneity.

Acknowledgements

The research reported in this publication was supported by funding from King Abdullah University of Science and Technology (KAUST). The authors would like to thank Sergey Borisov for providing the optode material.

References

[1] S.S. Branda, A. Vik, L. Friedman, R. Kolter, Biofilms: the matrix revisited, Trends Microbiol., 13 (2005) 20–26.
[2] J.W. Costerton, Z. Lewandowski, D.E. Caldwell, D.R. Korber, H.M. Lappin-Scott, Microbial biofilms, Annu. Rev. Microbiol., 49 (1995) 711–745.
[3] A.I. Radu, J.S. Vrouwenvelder, M.C.M. van Loosdrecht, C. Picioreanu, Effect of flow velocity, substrate concentration and hydraulic cleaning on biofouling of reverse osmosis feed channels, Chem. Eng. J., 188 (2012) 30–39.

[4] O.E. Petrova, K. Sauer, Sticky situations: key components that control bacterial surface attachment, J. Bacteriol., 194 (2012) 2413–2425.
[5] A.I. Radu, M.S.H. van Steen, J.S. Vrouwenvelder, M.C.M. van Loosdrecht, C. Picioreanu, Spacer geometry and particle deposition in spiral wound membrane feed channels, Water Res., 64 (2014) 160–176.
[6] L.F. Greenlee, D.F. Lawler, B.D. Freeman, B. Marrot, P. Moulin, Reverse osmosis desalination: water sources, technology, and today's challenges, Water Res., 43 (2009) 2317–2348.
[7] J.S. Baker, L.Y. Dudley, Biofouling in membrane systems – a review, Desalination, 118 (1998) 81–89.
[8] M. Herzberg, M. Elimelech, Biofouling of reverse osmosis membranes: role of biofilm-enhanced osmotic pressure, J. Membr. Sci., 295 (2007) 11–20.
[9] C.P. Koutsou, S.G. Yiantsios, A.J. Karabelas, A numerical and experimental study of mass transfer in spacer-filled channels: effects of spacer geometrical characteristics and Schmidt number, J. Membr. Sci., 326 (2009) 234–251.
[10] B. Gu, C.S. Adjiman, X.Y. Xu, The effect of feed spacer geometry on membrane performance and concentration polarisation based on 3D CFD simulations, J. Membr. Sci., 527 (2017) 78–91.
[11] H.C. Flemming, Biofouling in water systems – cases, causes and countermeasures, Appl. Microbiol. Biotechnol., 59 (2002) 629–640.
[12] J. Baker, T. Stephenson, S. Dard, P. Cote, Characterization of fouling of nanofiltration membranes used to treat surface waters, Environ. Technol., 16 (1995) 977–985.
[13] T. Tran, B. Bolto, S. Gray, M. Hoang, E. Ostarcevic, An autopsy study of a fouled reverse osmosis membrane element used in a brackish water treatment plant, Water Res., 41 (2007) 3915–3923.
[14] B.B. Christensen, C. Sternberg, J.B. Andersen, R.J. Palmer, A.T. Nielsen, M. Givskov, S. Molin, Molecular tools for study of biofilm physiology, Methods Enzymol., 310 (1999) 20–42.
[15] S. West, M. Wagner, C. Engelke, H. Horn, Optical coherence tomography for the in situ three-dimensional visualization and quantification of feed spacer channel fouling in reverse osmosis membrane modules, J. Membr. Sci., 498 (2016) 345–352.
[16] N.M. Farhat, M. Staal, A. Siddiqui, S.M. Borisov, S.S. Bucs, J.S. Vrouwenvelder, Early non-destructive biofouling detection and spatial distribution: application of oxygen sensing optodes, Water Res., 83 (2015) 10–20.
[17] L. Fortunato, T. Leiknes, In-situ biofouling assessment in spacer filled channels using optical coherence tomography (OCT): 3D biofilm thickness mapping, Bioresour. Technol., 229 (2017) 231–235.
[18] A. Bridier, F. Dubois-Brissonnet, A. Boubetra, V. Thomas, R. Briandet, The biofilm architecture of sixty opportunistic pathogens deciphered using a high throughput CLSM method, J. Microbiol. Methods, 82 (2010) 64–70.
[19] C. Picioreanu, J.S. Vrouwenvelder, M.C.M. van Loosdrecht, Three-dimensional modeling of biofouling and fluid dynamics in feed spacer channels of membrane devices, J. Membr. Sci., 345 (2009) 340–354.
[20] G. Holst, O. Kohls, I. Klimant, B. Konig, M. Kuhl, T. Richter, A modular luminescence lifetime imaging system for mapping oxygen distribution in biological samples, Sens. Actuators, B, 51 (1998) 163–170.
[21] I. Klimant, M. Kuhl, R.N. Glud, G. Holst, Optical measurement of oxygen and temperature in microscale: strategies and biological applications, Sens. Actuators, B, 38 (1997) 29–37.
[22] R.N. Glud, M. Kuhl, O. Kohls, N.B. Ramsing, Heterogeneity of oxygen production and consumption in a photosynthetic microbial mat as studied by planar optodes, J. Phycol., 35 (1999) 270–279.
[23] M. Kuhl, L. Polerecky, Functional and structural imaging of phototrophic microbial communities and symbioses, Aquat. Microb. Ecol., 53 (2008) 99–118.
[24] D. Debeer, P. Stoodley, F. Roe, Z. Lewandowski, Effects of biofilm structures on oxygen distribution and mass-transport, Biotechnol. Bioeng., 43 (1994) 1131–1138.
[25] M. Staal, E.I. Prest, J.S. Vrouwenvelder, L.F. Rickelt, M. Kuhl, A simple optode based method for imaging O-2 distribution and dynamics in tap water biofilms, Water Res., 45 (2011) 5027–5037.
[26] R. Almstrand, H. Daims, F. Persson, F. Sorensson, M. Hermansson, New methods for analysis of spatial distribution and coaggregation of microbial populations in complex biofilms, Appl. Environ. Microb., 79 (2013) 5978–5987.
[27] H. Daims, M. Wagner, In situ techniques and digital image analysis methods for quantifying spatial localization patterns of nitrifiers and other microorganisms in biofilm and flocs, Methods Enzymol., 496 (2011) 185–215.
[28] J.S. Vrouwenvelder, S.M. Bakker, M. Cauchard, R. Le Grand, M. Apacandie, M. Idrissi, S. Lagrave, L.P. Wessels, J.A.M. van Paassen, J.C. Kruithof, M.C.M. van Loosdrecht, The membrane fouling simulator: a suitable tool for prediction and characterisation of membrane fouling, Water Sci. Technol., 55 (2007) 197–205.
[29] J.S. Vrouwenvelder, C. Hinrichs, W.G.J. Van der Meer, M.C.M. Van Loosdrecht, J.C. Kruithof, Pressure drop increase by biofilm accumulation in spiral wound RO and NF membrane systems: role of substrate concentration, flow velocity, substrate load and flow direction, Biofouling, 25 (2009) 543–555.
[30] S.M. Borisov, G. Nuss, I. Klimant, Red light-excitable oxygen sensing materials based on platinum(II) and palladium(II) benzoporphyrins, Anal. Chem., 80 (2008) 9435–9442.
[31] P. Stoodley, Z. Lewandowski, J.D. Boyle, H.M. Lappin-Scott, Oscillation characteristics of biofilm streamers in turbulent flowing water as related to drag and pressure drop, Biotechnol. Bioeng., 57 (1998) 536–544.
[32] S. Wasche, H. Horn, D.C. Hempel, Influence of growth conditions on biofilm development and mass transfer at the bulk/biofilm interface, Water Res., 36 (2002) 4775–4784.
[33] P. Stoodley, D. Debeer, Z. Lewandowski, Liquid flow in biofilm systems, Appl. Environ. Microb., 60 (1994) 2711–2716.
[34] C. Picioreanu, M.C.M. van Loosdrecht, J.J. Heijnen, Mathematical modeling of biofilm structure with a hybrid differential-discrete cellular automaton approach, Biotechnol. Bioeng., 58 (1998) 101–116.
[35] R.R. Sharp, P. Stoodley, M. Adgie, R. Gerlach, A. Cunningham, Visualization and characterization of dynamic patterns of flow, growth and activity of biofilms growing in porous media, Water Sci. Technol., 52 (2005) 85–90.
[36] H. Li, J.F. Reynolds, On definition and quantification of heterogeneity, Oikos, 73 (1995) 280–284.
[37] H. Beyenal, C. Donovan, Z. Lewandowski, G. Harkin, Three-dimensional biofilm structure quantification, J. Microbiol. Methods, 59 (2004) 395–413.
[38] L.A. Bereschenko, H. Prummel, G.J.W. Euverink, A.J.M. Stams, M.C.M. van Loosdrech, Effect of conventional chemical treatment on the microbial population in a biofouling layer of reverse osmosis systems, Water Res., 45 (2011) 405–416.

Supplementary material

Additional description image handling

Calculation of the standard deviation of the image. ImageJ can generate a standard deviation projection of the stack of 40 images, giving the standard deviation per pixel for the whole image. It can also calculate the standard deviation of all pixels in one image or even for the whole stack. The latter does not take into account that there is repetitive structuring within the images. Alternatively, the standard deviation can be calculated over the stack of the images as is described in (Eq. (1)) or it can be calculated for the variation of every single image compared with the average image. In the latter case an image in the stack is subtracted by the average image. The result image is then converted into an absolute value image. The average value of this image then can be used as the deviation of that image from the average value.

$$\sigma = \sqrt{\frac{1}{N}\sum_{i=1}^{N}(I_i - \bar{I})^2} \quad (1)$$

σ, standard deviation; N, total number of samples; I_i, value of sample number i; $\bar{I}$: average of all samples.

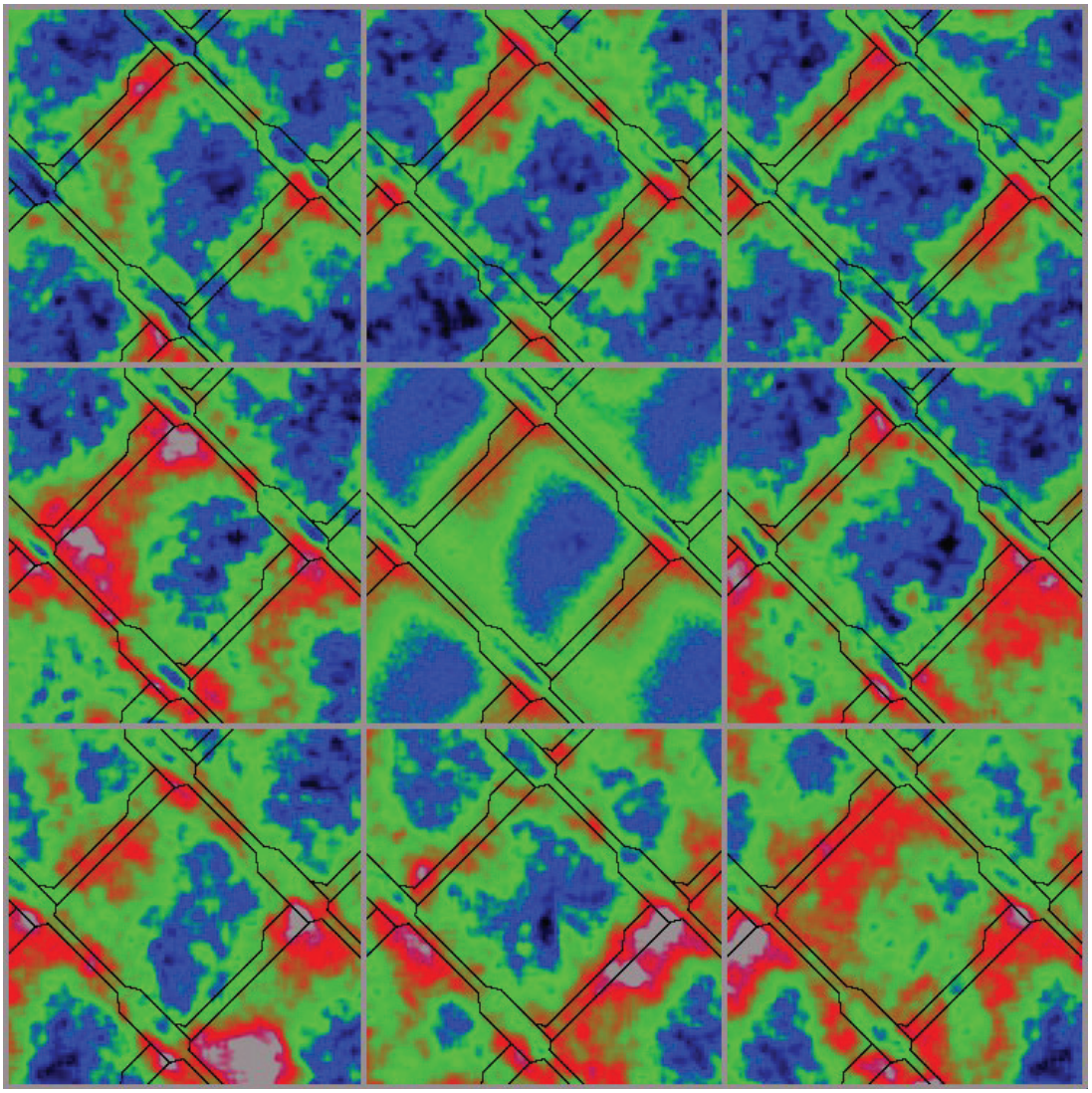

Fig. S1. Indication of the variation of single spacer frame images from the average ODR image at the outlet at a flow of 0.16 m s^{-1}. The image in the centre is the average image of 40 spacer frames. The images around are the individual images after filtering with mean filter (1 pixels).